Science of the Total Environment 917 (2024) 170485

Contents lists available at ScienceDirect

Science of the Total Environment

journal homepage: www.elsevier.com/locate/scitotenv

Trends and drivers of aerosol vertical distribution over China from 2013 to 2020: Insights from integrated observations and modeling

Xi Chen [a], Ke Li [a,*], Ting Yang [b], Zhenjiang Yang [a], Xueqing Wang [a], Bin Zhu [c], Lei Chen [a], Yang Yang [a], Zifa Wang [b], Hong Liao [a]

[a] Joint International Research Laboratory of Climate and Environment Change, Jiangsu Key Laboratory of Atmospheric Environment Monitoring and Pollution Control, Collaborative Innovation Center of Atmospheric Environment and Equipment Technology, School of Environmental Science and Engineering, Nanjing University of Information Science and Technology, Nanjing 210044, China

[b] State Key Laboratory of Atmospheric Boundary Layer Physics and Atmospheric Chemistry (LAPC), Institute of Atmospheric Physics, Chinese Academy of Sciences, Beijing 100029, China

[c] Collaborative Innovation Center on Forecast and Evaluation of Meteorological Disasters, Key Laboratory for Aerosol-Cloud-Precipitation of China Meteorological Administration, Nanjing University of Information Science & Technology, Nanjing 210044, China

HIGHLIGHTS

- The seasonality and spatiality of 8-year satellite AOD trends can be reasonably reproduced by long-term model simulation.
- Emission reduction dominated the decline in AOD, and the meteorology contribution varied seasonally.
- Aerosol extinction coefficient decreased by −8.0 %/yr to -5.5 %/yr below ~1 km, determined by emission reduction, PBLH, and RH.
- Sulfate contributed to 50% AOD decline in summer, while organic aerosol contribution doubled to 24%–35% in winter.

GRAPHICAL ABSTRACT

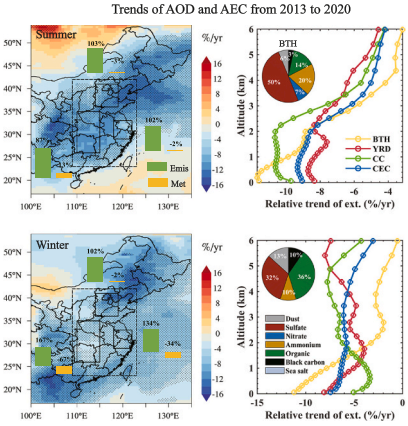

ARTICLE INFO

Editor: Jianmin Chen

Keywords:
Aerosol vertical distribution
Aerosol optical depth
Clean air actions
China
GEOS-Chem

ABSTRACT

Understanding aerosol vertical distribution is of great importance to climate change and atmospheric chemistry, but there is a dearth of systematical analysis for aerosol vertical distribution amid rapid emission decline after 2013 in China. Here, the GEOS-Chem model and multiple-sourced observations were applied to quantify the changes of aerosol vertical distributions in response to clean air actions. In 2013–2020, the MODIS aerosol optical depth (AOD) presented extensive decreasing trends by −7.9 %/yr to −4.2 %/yr in summer and −6.1 %/yr to −5.8 %/yr in winter in polluted regions. Vertically, the aerosol extinction coefficient (AEC) from CALIPSO decreased by −8.0 %/yr to −5.5 %/yr below ~1 km, but the trends weakened significantly with increasing altitude. Compared with available measurements, the model can reasonably reproduce 2013–2020

* Corresponding author.
E-mail address: keli@nuist.edu.cn (K. Li).

https://doi.org/10.1016/j.scitotenv.2024.170485
Received 1 December 2023; Received in revised form 21 January 2024; Accepted 24 January 2024
Available online 29 January 2024

trends and seasonality in AOD and vertical AEC. Model simulations confirm that emission reduction was the dominant driver of the 2013–2020 decline in AOD, while the effect of meteorology varied seasonally, with contributions ranging from −2 % to 13 % in summer and −67 % to −2 % in winter. Vertical distributions of emission-driven AEC trends strongly depended on emission reductions, local planetary boundary layer height, and relative humidity. For aerosol components, sulfate accounted for ~50 % of the AOD decline during summer, followed by ammonium and organic aerosol, while in winter the contribution of organic aerosol doubled (24 %–35 %), and nitrate exhibited a weak increasing trend. Chemical production and meteorological conditions (e.g., relative humidity) primarily drove the nitrate contribution, but emission reduction and hygroscopicity were decisive for other components. This work provides an integrated observational and modeling effort to better understand rapid changes in aerosol vertical distribution over China.

1. Introduction

The vertical distribution of aerosols plays a key role in both climate change and atmospheric chemistry. The climate sensitivity (Zhang et al., 2017) and radiative effects (Yu et al., 2019) of aerosols are closely dependent on their vertical profiles. For example, absorbing and scattering aerosols can have opposite climate effects at different altitudes (Ma et al., 2022). Understanding the vertical distribution characteristics of aerosols is essential for assessing their impact on climate change (Wang et al., 2016). More importantly, aerosols, as the most-concerned air pollutant, can be transported regionally (Huang et al., 2020) or even globally (Uno et al., 2009; Sokolik et al., 2019). By quantifying the vertical distribution of aerosols, it is possible to identify transport pathways (Prospero et al., 2020) and pollution sources (Wu et al., 2017), in particular for regional air pollution issues. Furthermore, the radiative effects of aerosols could worsen air quality through aerosol-boundary layer interactions (Ding et al., 2016), which is also closely related to aerosol vertical distribution (Ma et al., 2022).

To address severe fine particulate matter ($PM_{2.5}$) pollution, the Chinese government has promulgated a series of strict emission control policies since 2013, including the Air Pollution Prevention and Control Action Plan (2013–2017) and the following Three-year Action Plan for Blue Sky Defense (2018–2020). With anthropogenic emissions markedly reduced (Zheng et al., 2018), there were rapid nationwide declines in $PM_{2.5}$ concentrations (Zhang et al., 2019; Xiao et al., 2022). Numerous studies have characterized the variation of aerosol concentrations at the surface from the perspective of spatial and temporal distribution (Wang et al., 2017), components (Lei et al., 2021), sources (Deng et al., 2022), and drivers (Chen et al., 2019; Dang and Liao, 2019). However, there is much less attention paid to the changes in the vertical distribution of aerosols.

Satellite observations are typically employed for studying long-term vertical distribution of aerosols. The Cloud-Aerosol Lidar and Infrared Pathfinder Satellite Observations (CALIPSO) data have been extensively utilized in China (Reddy et al., 2019; Su et al., 2020; Gui et al., 2021; Liao et al., 2021; Chen et al., 2023a). Based on long-term CALIPSO observations, Gui et al. (2021) examined the 2007–2019 trends of column AOD in various altitude regimes across the globe and their analysis revealed precipitation, soil moisture, and wind speed as driving factors of AOD trends based on correlation analysis. Chen et al. (2023a) analyzed the CALIPSO AOD trends in nine regions of China from 2006 to 2020 and discussed the vertical distribution and transport pathways of different aerosols. These studies paid little attention to the period with rapid aerosol changes after clean air actions. In our previous study, the annual variations and drivers of aerosol vertical distribution in typical polluted regions after 2013 were revealed based on 7-year observations from CALIPSO (Chen et al., 2023b). Recently, Liu et al. (2023) examined the aerosol responses to anthropogenic emission reduction over North China using multiple observational measurements. They identified the seasonal differences in AOD trends after 2013, while previous studies primarily focused on long-term average (Li et al., 2022) or trends of annual average (Guo et al., 2016; Chen et al., 2022a; Chen et al., 2023b). Although the role of emission and meteorology changes has been explored in previous studies, it is challenging to understand their contributions or characterize the changes in aerosol chemical components based only on observational and statistical analysis.

The chemical transport modeling (CTM) can provide a quantitative analysis of aerosol vertical distribution. The ability of CTM to replicate the vertical distribution of aerosols has been demonstrated through comparisons with various observations, including Unmanned Aerial Vehicles (Liu et al., 2021), CALIPSO observation (Li and Han, 2016; Ma et al., 2021), radiosonde data (Lu et al., 2023), and aircraft measurements (Zhai et al., 2021b; Chen et al., 2022b). Previous modeling studies primarily focused on individual pollution episodes. For example, Lu et al. (2023) employed WRF-Chem coupled with a tagging method to assess the influence of regional transport on the vertical distribution of black carbon during typical pollution episodes in eastern China. Kang et al. (2022) investigated the effects of a strong urban heat island process on the vertical distribution of inorganic aerosol in Hangzhou using the WRF-CMAQ model. However, long-term simulations of the aerosol vertical distribution are limited, and most of the early studies investigated the long-term variations in AOD (Li et al., 2013; Li and Han, 2016). Ma and Yu (2014) and Li et al. (2019b) analyzed long-term aerosol vertical profiles before 2014 in Europe, the US, and China, respectively, utilizing numerical models with CALIPSO observations. Therefore, there is still a lack of quantitative understanding of aerosol vertical distribution after the clean air actions in China.

Built on our previous observational study (Chen et al., 2023b), herein, we integrated the Goddard Earth Observing System Chemical Transport Model (GEOS-Chem) and multiple observational datasets to quantify the trends of aerosol vertical distributions in China after clean air actions (2013–2020). We presented not only the annual but also the seasonal features of the long-term trends of AOD and aerosol vertical distribution over eastern China, including three heavily polluted city clusters. Furthermore, we quantified the effects of emission controls and meteorological changes by conducting sensitivity simulations. We also identified the drivers of aerosol vertical distribution in response to emission controls, considering the role of aerosol components and meteorological factors. Our findings provide a quantitative understanding of the factors driving aerosol vertical distribution over China amid fast-changing emission reductions.

2. Data and methods

2.1. Observations

To investigate the long-term trends of aerosol vertical distribution, both active and passive remote sensing data were used in this study (Table 1). The Level 3 monthly average AOD data (MYD08_M3) at 550 nm obtained from Moderate Resolution Imaging Spectroradiometer (MODIS) Collection 6.1 (C6.1) products were used to evaluate trends of AOD. The AOD data retrieved with the Dark Target and Deep Blue combined algorithms cover 8 years (2013–2020) and have a horizontal resolution of $1^\circ \times 1^\circ$. Vertical distributions of aerosol extinction coefficient (AEC) trends were analyzed based on the CALIPSO Level 2 aerosol profile product (V4.20). The product provides profiles of AECs at 532 nm with a horizontal resolution of 5 km and a vertical resolution of 60 m. Although solar background illumination can cause systematic

Table 1
Surface and satellite observations used in this work.

Variable	Data source	Time
Monthly average AOD data at 550 nm	MODIS Collection 6.1 Level 3	2013–2020
Profiles of aerosol extinction coefficient at 532 nm	CALIPSO V4.20 Level 2	2013–2020
Hourly surface $PM_{2.5}$ concentrations	Ministry of Ecology and Environment	2013–2020
Profiles of aerosol extinction coefficient at 532 nm	Ground-based lidar in IAP	2017

biases during the daytime, both daytime and nighttime data were considered because this work focuses on long-term trends. We conducted serials of quality control procedures to reduce the unreliability of CALIPSO data, and all data below 120 m were excluded due to the great uncertainty in CALIPSO observations near the surface (Wang et al., 2016). The filtering criteria referred to the official website and our previous study (Chen et al., 2023b).

To evaluate model performance, long-term hourly surface $PM_{2.5}$ concentrations from the Ministry of Ecology and Environment (MEE) network and one year (2017) of AEC data from a ground-based Mie-scattering lidar in Beijing were used. The $PM_{2.5}$ concentrations from MEE are available after April 2013 and can be archived at http://quotsoft.net/air (Wang, 2023). The ground-based lidar is in the Institute of Atmospheric Physics, Chinese Academy of Sciences (39.982°N, 116.385°E), with a wavelength of 532 nm and a vertical resolution of 30 m. The data quality control scheme was implemented for the lidar observation, and more details can be found in Wang et al. (2020).

2.2. GEOS-Chem simulation

We used the GEOS-Chem model version 13.3.3 for the long-term air quality simulation over China (15–55°N, 70–140°E). The model was driven by the MERRA-2 meteorological data from NASA with a horizontal resolution of 0.5° × 0.625° and 47 vertical layers. A global simulation with a horizontal resolution of 2° × 2.5° provided the chemical boundary conditions for the nested-grid simulation every 3 h. GEOS-Chem has been widely applied to simulate the $PM_{2.5}$ air quality in China (Yang et al., 2016; Li et al., 2021; Zhai et al., 2021a; Tan et al., 2023). Herein, the boundary layer mixing, dry deposition, and wet deposition schemes followed the configuration in Zhai et al. (2021b). AOD at 550 nm in GEOS-Chem was summed up by aerosol components including sulfate–nitrate–ammonium (SNA), organic aerosol (OA), black carbon (BC), sea salt (SA), and dust. Detailed descriptions for the calculation of aerosol optical properties are given in Drury et al. (2010) and Zhai et al. (2021b). As sulfate, nitrate, and ammonium share the same aerosol optical properties in GEOS-Chem, we separated the AOD of SNA according to their mass concentrations.

We performed two 8-year simulations to quantify the contribution of changed meteorological conditions and emission controls implemented by clean air actions. The baseline simulation was driven by changing emissions and meteorology from 2013 to 2020, from which the simulated trends of aerosol vertical distribution can be derived. The sensitivity simulation was conducted with fixed anthropogenic emissions in 2013 and varying meteorological conditions, from which the trends contributed by meteorological variations can be derived. Emission-driven trends can be separated by comparing the trends between baseline simulation and sensitivity simulation. In addition, we also calculated the relative contributions of emission controls and meteorological variations, respectively, to the simulated overall trends from the baseline simulation. Anthropogenic emissions from 2013 to 2020 are from the Multiresolution Emission Inventory for China (MEIC), which can be accessed at http://www.meicmodel.org. In addition, we took biomass burning emissions and biogenic emissions from the Global Fire Emissions Database version 4 (GFED4) and MEGANv2, respectively (Guenther et al., 2012; van der Werf et al., 2017). Other natural emissions were configured as the same with Li et al. (2021).

3. Results and discussion

3.1. Observed long-term trends in AOD and aerosol vertical distribution

We focused on Central and Eastern China (CEC, 23–42°N, 109–123°E) where severe aerosol pollution was observed (Fig. S1). The long-term trends in AOD were determined by calculating the linear regression coefficient of annual time series and the *t*-test was used to determine whether the derived trend is statistically significant. From 2013 to 2020, it witnessed a notable decline in AOD from MODIS over the CEC region (−0.25 decade^{-1}). The absolute trends of annual mean AOD (Fig. S2) were stronger in heavily polluted city clusters, like Beijing-Tianjin-Hebei (BTH), the Yangtze River Delta (YRD), and Central China (CC). In Table 2, the observed annual mean AOD exhibited the fastest decline in the BTH (−0.41 decade^{-1}), followed by the CC (−0.35 decade^{-1}) and YRD (−0.30 decade^{-1}). Compared to the AOD trend of approximately −0.2 decade^{-1} for the period of 2007–2019 in the CEC region (Gui et al., 2021), the decline in AOD was accelerated following the implementation of clean air actions.

Fig. 1 shows that the absolute trends of AOD from MODIS exhibited an obvious seasonality. In summer, the MODIS AOD exhibited the most rapid decline in the BTH region (−0.53 decade^{-1}); however, in winter, the differences between regions diminished, and the most significant decline occurred in the YRD. In spring and autumn (Fig. S3), the decline in AOD exhibited a slower trend, with the most rapid decline in the CC region (−0.37 decade^{-1}) and BTH region (−0.33 decade^{-1}), respectively. Consequently, our focus shifted to the seasonality of trends in the aerosol vertical distribution in summer and winter when the decline of AOD is faster and the spatial variability is greater. Specifically, the decline of AOD in the BTH and CC regions was faster by a factor of 1.4 in summer compared to winter. Liu et al. (2023) also reported a similar seasonal feature in AOD trends over 2013–2019 in Northern China based on two MODIS datasets. For the YRD region, in contrast, the regional mean AOD declined by −0.40 decade^{-1} in winter, which was 1.5 times faster than that in summer. Overall, the AOD trend for the whole CEC region was −0.23 decade^{-1} in summer and − 0.20 decade^{-1} in winter (Table 2). In the downwind region of mainland China, there was a negative trend over the western Pacific during winter while the negative trend only covered the north part of 30°N during summer, which could be attributed to the seasonal shift in wind direction related to East Asia monsoon.

Figs. 2a-b illustrate the spatial distributions of relative AOD trends from MODIS during summer and winter. The seasonality of relative trends was weaker than absolute trends and this is supported by the

Table 2
Regionally averaged relative trends (%/yr) and absolute trends (decade^{-1}, in brackets) of AOD during 2013–2020 from MODIS and the GEOS-Chem (GC) simulation. Trends marked with asterisks are statistically significant based on the *t*-test ($p < 0.05$). The "Annual" represents the annual (all seasons) mean AOD trends.

			BTH	YRD	CC	CEC
AOD	JJA	MODIS	−6.8 (−0.53) *	−4.2 (−0.30)	−7.9 (−0.42)	−4.3 (−0.23)
		GC	−9.2 (−0.56) *	−8.0 (−0.24)	−10.0 (−0.34)	−8.4 (−0.30) *
	DJF	MODIS	−5.8 (−0.38)	−6.1 (−0.40)	−5.9 (−0.31) *	−4.4 (−0.20)
		GC	−8.1 (−0.31) *	−6.1 (−0.26) *	−4.3 (−0.26) *	−6.4 (−0.24) *
	Annual	MODIS	−6.0 (−0.41) *	−5.0 (−0.30) *	−6.5 (−0.35) *	−5.0 (−0.25) *
		GC	−9.0 (−0.43) *	−6.9 (−0.25) *	−6.5 (−0.31) *	−7.3 (−0.26) *

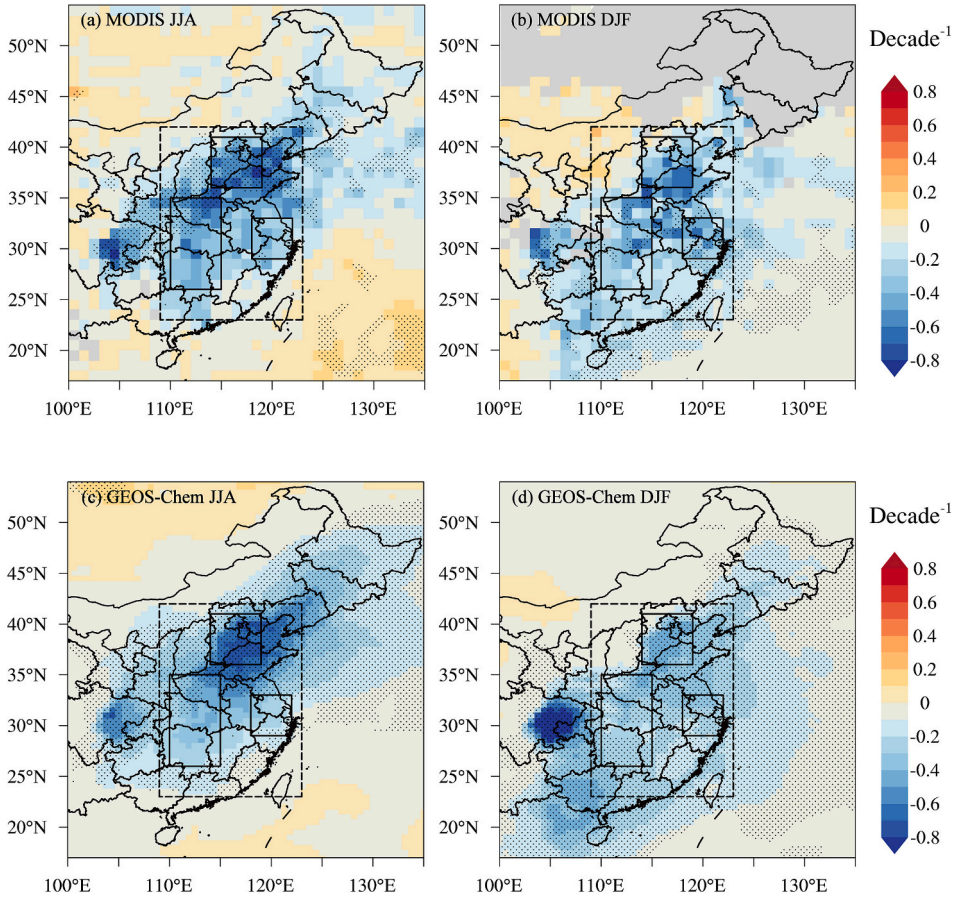

Fig. 1. Seasonality of absolute trends of AOD during 2013–2020 from (a-b) MODIS and (c-d) the GEOS-Chem simulation. Dotting indicates trends are statistically significant based on the *t*-test ($p < 0.05$). The dashed rectangle represents Central and Eastern China (CEC, 23–42°N, 109–123°E). The three solid rectangles represent distinct regions: Beijing-Tianjin-Hebei (BTH, 36–41°N, 114–119°E), the Yangtze River Delta (YRD, 29–33°N, 118–122°E), and Central China (CC, 26–35°N, 110–115°E).

estimated AOD trend of −4.3 %/yr in summer and of −4.4 %/yr in winter over the CEC (Table 2). Regionally, the mean AOD during summer declined by −6.8 %/yr and − 7.9 %/yr in the BTH and CC region, respectively, which was 1.2–1.3 times higher than the decline in winter. Similar to absolute trends, the relative decreasing trend of AOD by −6.1 %/yr in the YRD region was about 1.5 times higher in winter than in summer. Unlike the absolute trend, the relative decreasing trend of AOD from MODIS was more significant in the CC region than in other regions in summer and the regional difference in relative trends was smaller in winter.

AOD characterizes the vertical distribution of aerosols throughout the atmospheric column, and the AOD trends can vary significantly across different altitude levels (Gui et al., 2021). Therefore, we further explored the long-term trends of aerosol vertical distribution based on CALIPSO data. Fig. 3a shows vertical profiles of the relative trends of annual mean AEC over 2013–2020. In the near-surface layer, the relative trends in BTH, YRD, CC, and CEC were about −8.0 %/yr, −6.0 %/yr, −5.5 %/yr, and −5.5 %/yr, respectively. With increasing altitude, the decreasing trends in AEC slowed down and this characteristic was more prominent in the BTH region. The decreasing trend in the YRD region was only statistically significant ($p < 0.05$) below 1 km, while the significant decrease can extend up to 3 km in other regions. Due to the long transit period of CALIPSO, the trends by season were not statistically significant with limited profiles. Therefore, the seasonality in relative trends of aerosol vertical distribution will be discussed based on model results.

3.2. Simulated long-term trends in AOD and aerosol vertical distribution

The GEOS-Chem model has been widely used in air quality research globally and well validated against multiple-sourced measurements for aerosols in China (Li et al., 2019a; Sun et al., 2021; Zhai et al., 2021a; Qi et al., 2022). However, the long-term aerosol trends and vertical aerosol profiles are few evaluated. Here we evaluated the GEOS-Chem model by using the surface $PM_{2.5}$ measurement, lidar observation, and satellite AOD. In Fig. 4, we compared the monthly mean surface $PM_{2.5}$ concentrations between simulations and observations for the focused regions. The GEOS-Chem model tended to overestimate $PM_{2.5}$ concentrations, with the normalized mean bias (NMB) of 16.6 % for the BTH region and of 33.2 % for the CC region. Nevertheless, the model successfully captured the long-term changes in $PM_{2.5}$ concentration, demonstrating a correlation coefficient of 0.94–0.95 and a normalized mean squared error (NMSE) of 0.18–0.37 across different regions. More importantly, the observed relative trends of annual $PM_{2.5}$ concentrations over 2014–2020 were well reproduced by the long-term GEOS-Chem simulations. The model only tended to underestimate the observed trends for different regions by 1 % to 8 %.

We also compared the AOD from MODIS and GEOS-Chem for summer and winter, respectively (Fig. S4). The model results were interpolated to match the MODIS grid to enable a matching comparison. Although there was no underestimation in aerosol mass during summer, the model consistently underestimated the observed AOD for different years, with the slopes of linear regression ranging from 1.24 (2015) to 1.64 (2020). The underestimation of AOD makes the relative trends from the model stronger in summer. In winter, the slopes of linear

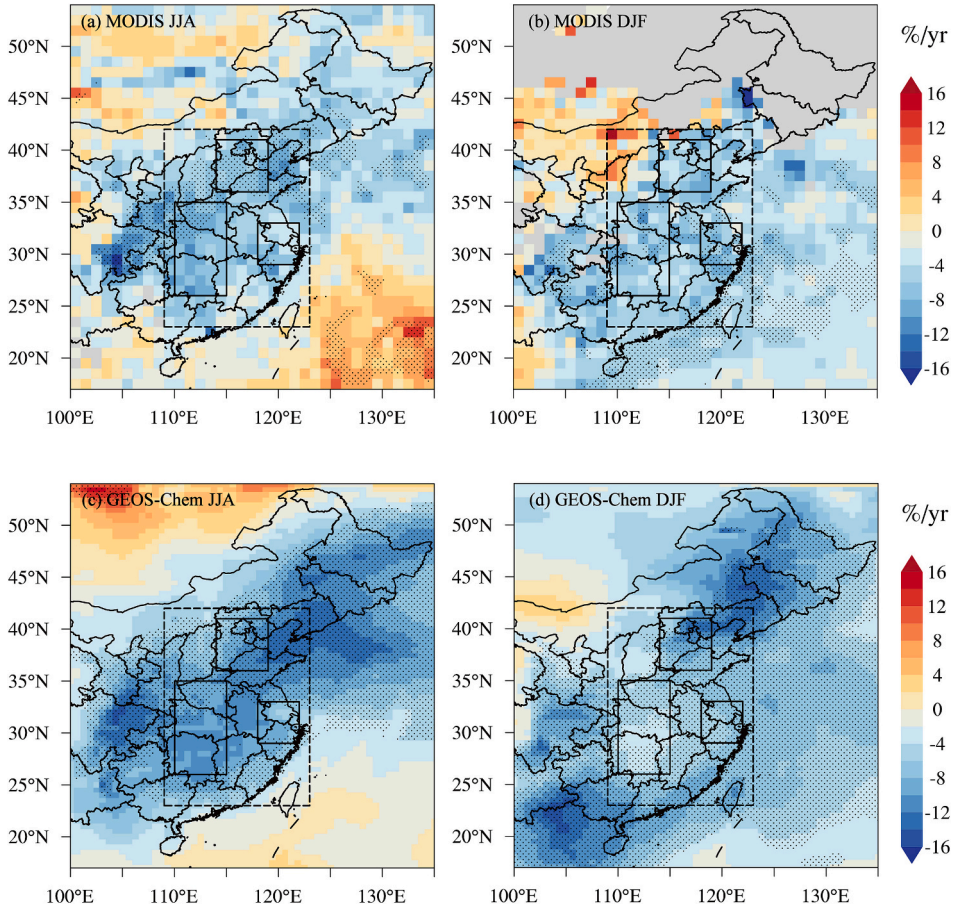

Fig. 2. Same as Fig. 1 but for the relative trends (%/yr) from (a-b) MODIS and (c-d) the GEOS-Chem simulation.

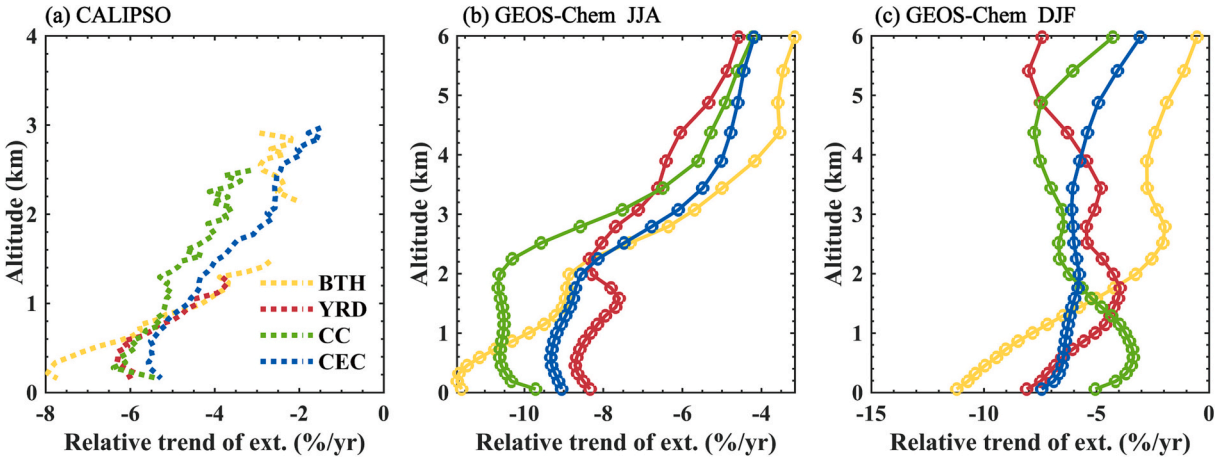

Fig. 3. (a) Vertical profiles of relative trends of annual mean aerosol extinction coefficient (AEC) during 2013–2020 from CALIPSO data. Only observed trends with statistical significance of $p < 0.05$ are given. (b-c) Vertical profiles of relative trends of seasonal mean AEC from the GEOS-Chem simulation.

regression ranged from 0.90 (2017) to 1.06 (2020), indicating no evident model bias for AOD. Previous studies utilizing GEOS-Chem in both China and the United States have also reported these similar seasonal biases in simulated AOD (Kim et al., 2015; Lin and Li, 2016; Zhai et al., 2021b). The low bias of MERRA2 relative humidity (RH) in summer (Fig. S5) can be one of the important factors to blame for this model error. Secondly, the more representative aerosol optical properties for China could reduce the error of model simulation (Zhai et al., 2021b). In addition, errors in model aerosol sources (Kim et al., 2015) and sampling differences between MODIS and simulations (Lin and Li, 2016) can also cause some uncertainty.

Fig. 5 shows the performance of GEOS-Chem in reproducing the observed vertical distribution of aerosols from continuous one-year observations by ground-based lidar in 2017 in Beijing. The model exhibited underestimation of the AEC in the lower atmosphere (~190 m) during both summer and winter, with 27 % and 34 %, respectively. The model consistently underestimated the extinction coefficient at all levels in winter, and the underestimation was decreased to

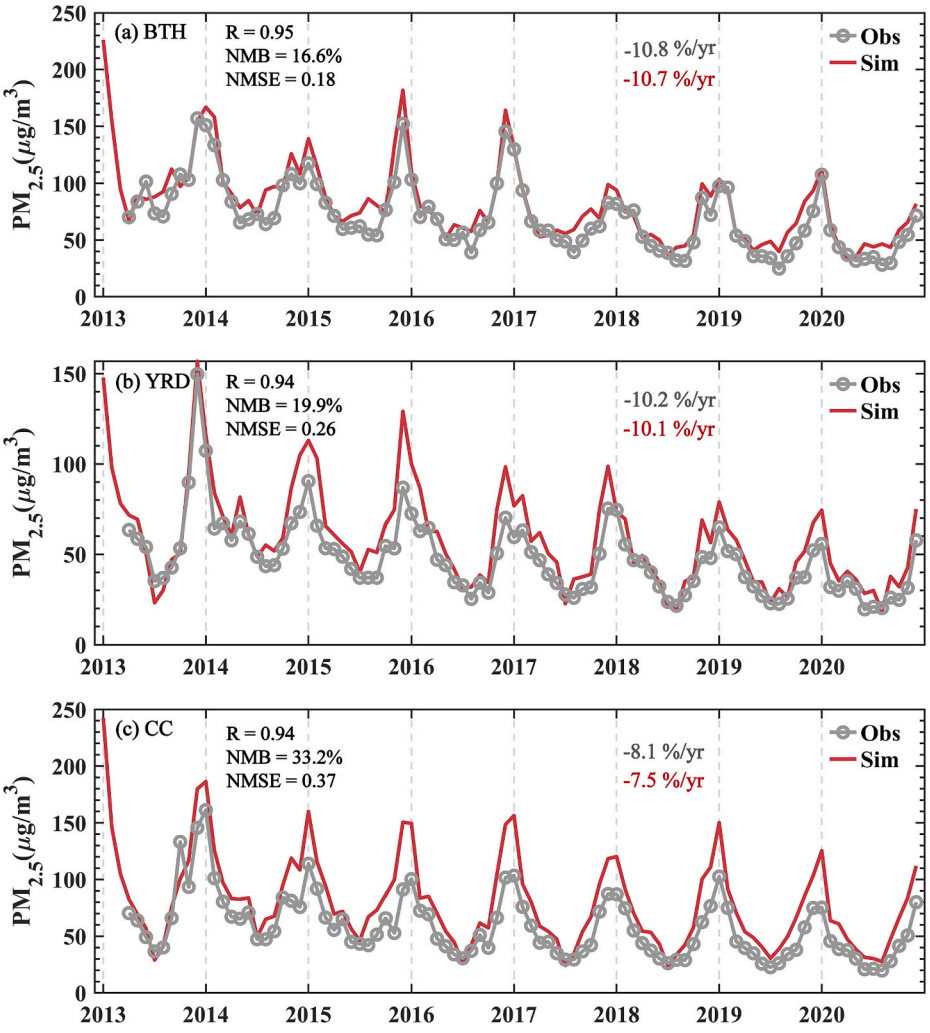

Fig. 4. Comparison of simulated (red) and observed (grey) monthly $PM_{2.5}$ concentrations averaged over (a) Beijing-Tianjin-Hebei (BTH), (b) the Yangtze River Delta (YRD), and (c) Central China (CC) from 2013 to 2020. Relative trends over 2014–2020 for annual $PM_{2.5}$ from observations (grey) and the model (red) are also inserted.

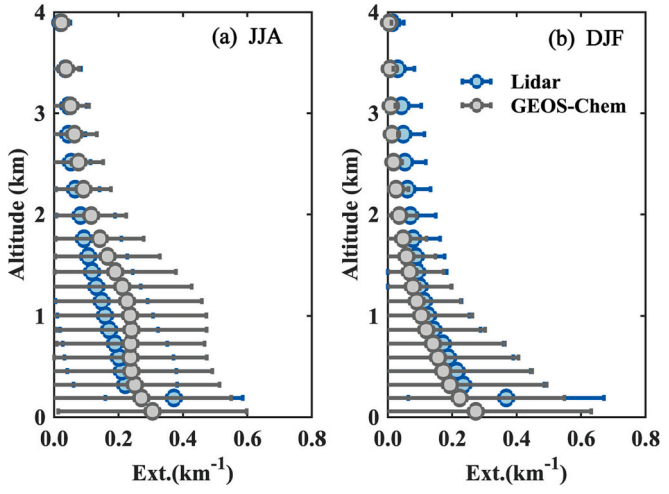

Fig. 5. The mean aerosol extinction coefficient profiles for (a) summer and (b) winter 2017 from the GEOS-Chem model and ground-based lidar at Beijing. Horizontal bars are standard deviations.

approximately 10 % within 1.5 km. As previously mentioned, the bias in RH can be an important factor contributing to the underestimation of the AEC (Zhai et al., 2021b). The daily average RH from the MERRA2 meteorological data was approximately 10 % lower than that of the ERA5 reanalysis data (Hersbach et al., 2020) at 1000 hPa, especially under high-RH conditions (Fig. S5). However, the RH values from the two datasets were close at 850 hPa, which could potentially account for the more obvious underestimation of the extinction coefficient occurred in the lower atmosphere. Li et al. (2019b) compared the vertical distribution of AECs obtained from CALIPSO and GEOS-Chem in northern China, and they also confirmed the model's underestimation of the extinction coefficient in winter. Conversely, GEOS-Chem overestimated the extinction coefficient at higher altitudes in summer, which is more consistent with the average profile derived from CALIPSO in the BTH region (Chen et al., 2023b).

For the long-term trends, a good agreement was observed between the MODIS data and GEOS-Chem simulation regarding the spatial distribution (see Figs. S2a-b) and the absolute trends of annual mean AOD (Table 2). The differences between the simulated and observed absolute annual trends were − 0.02 decade^{-1}, 0.05 decade^{-1}, and 0.04 decade^{-1} for BTH, YRD, and CC, respectively. The seasonality of absolute trends in AOD can also be found in the modeling results (Figs. 1c-d). The simulated AOD exhibited the fastest decline in the BTH region during both summer (−0.56 decade^{-1}) and winter (−0.31 decade^{-1}), followed by

the CC region. The decline of AOD in the BTH and CC regions was faster in summer compared to winter by a factor of 1.8 and 1.3, respectively. In the YRD region, the regional mean AOD declined faster in winter, which was also consistent with the observed results. However, the relative decreasing trends of seasonal mean AOD from the model tended to be faster than observations (Figs. 2c-d). For example, the simulated annual trend of AOD over CEC was −7.3 %/yr and it was only −5.0 %/yr from MODIS (Table 2). This could be mainly attributed to the underestimation of mean AOD levels in the model (Fig. S4), as the low bias of mean AOD and high bias of relative trend for AOD were both remarkable in summer.

Figs. 3b-c present the vertical distributions of relative trends of AEC in summer and winter. Consistent with the relative trends observed by CALIPSO, the decreasing trends of AEC in the BTH region were the fastest at lower altitudes, which then decelerated appreciably with increasing altitude in both summer and winter. Seasonally, in summer, the relative trends of AEC within 2 km showed smaller variations in the CC (−10.5 %/yr) and CEC (−9.0 %/yr) regions. Consequently, the decreasing trend of column AOD in the CC region was faster than that in BTH, despite the lower declining trends in the surface layer. In winter, the relative trends of AEC in the BTH region slowed down from −11.2 %/yr to −2.0 %/yr as altitude increased from the surface to ~3 km, which was more significant compared to summer (from −11.6 %/yr to −6.4 %/yr). These findings align with the results reported by Liu et al. (2023) based on the CALIPSO data over Northern China. In the CC and YRD regions, the decreasing trends of AEC reached the slowest point at approximately 0.6 km and 1.8 km, respectively. Contrary to summer, the relative trends of AEC in each region differed significantly at higher altitudes. Overall, against available measurements, the GEOS-Chem model simulated reasonable long-term trends in surface $PM_{2.5}$, column AOD, as well as vertical AECs over China in response to strict emission controls.

3.3. Quantified contributions by emission controls and meteorological variations

3.3.1. Drivers of 2013–2020 changes in AOD

Fig. 6 shows the spatial distributions of the relative trends of AOD attributed to emission controls. For the whole CEC region, the emission-driven trends were − 7.8 %/yr and − 6.7 %/yr in summer and winter, respectively. The decreasing trends of AOD in the YRD region were comparable between summer and winter, with a decrease of approximately −8.0 %/yr. In other regions, the decreasing trends driven by emission reduction were faster in summer than in winter, with a ratio of 1.2 to 1.3. This indicates that the seasonality of emission-driven trends was weaker than the seasonality of the overall trends. Similar to Fig. 2, the decreasing trends attributed to emission controls in winter extended to the whole downwind region of China, possibly due to the prevailing northwesterly winds during winter.

Fig. S6 gives the contribution of emission controls to the simulated declining trends of AOD. Consistent with previous studies on the drivers of $PM_{2.5}$ reduction (Zhang et al., 2019; Shao et al., 2023), the decline of AOD was also primarily driven by emission controls. In summer, the contribution of emission controls in the CC region was the lowest at 87 %, while in other regions, the contribution was approximately 100 %. This indicates that summer meteorological variations were favorable for the 2013–2020 decline of AOD in CC, and their impact on other regions can be neglected. In contrast, meteorological variations were not conducive to the decrease of AOD in winter. The contribution of emission controls in the YRD, CC, and CEC regions was estimated to be 134 %, 167 %, and 119 %, respectively. This means that although the primary factor for the whole CEC region was emission controls, meteorology could play an important role in the declining AOD trends over the CC region.

Then we further discussed the changes of aerosol components in response to emission controls. The model performance of GEOS-Chem in simulating major aerosol compositions over China has been validated by previous studies (Zhang et al., 2015; Miao et al., 2020; Zhai et al., 2021a). The long-existing issue that the model has a low bias in sulfate and a high bias in nitrate could be improved by updated heterogeneous sulfate production and wet scavenging scheme. This improvement has been demonstrated by Zhai et al. (2021a) based on abundant observational data. The model performance in SNA was first validated by comparing it with observations from 2013 to 2020 in Beijing (Lei et al., 2021). Regardless of dust, the modeled proportion of SNA in $PM_{2.5}$ was 31 % to 42 % in the cold season, about 10 % lower than the observed. Besides, we compared the monthly mean nitrate at Nanjing with the results of Zhai et al. (2021a) and it showed a good agreement with both the observations and the model results (not shown). As we followed their model configuration, we believe that the simulation of other aerosol components is reliable.

Fig. 7 shows that the contributions of aerosol components to the emission-driven declining trends of AOD exhibited distinct seasonality. In summer, sulfate dominated the reduction of AOD in different regions, with the contribution ranging from 47 % to 50 %, followed by ammonium and OA. Similarly, observations conducted in Beijing revealed a much greater decrease in SNA concentration compared to OA (Li et al., 2023), supporting the dominant role of SNA in AOD trend during summer. In winter, sulfate remained its dominant role but its contribution decreased by 18 % in the BTH relative to summer and the contribution of

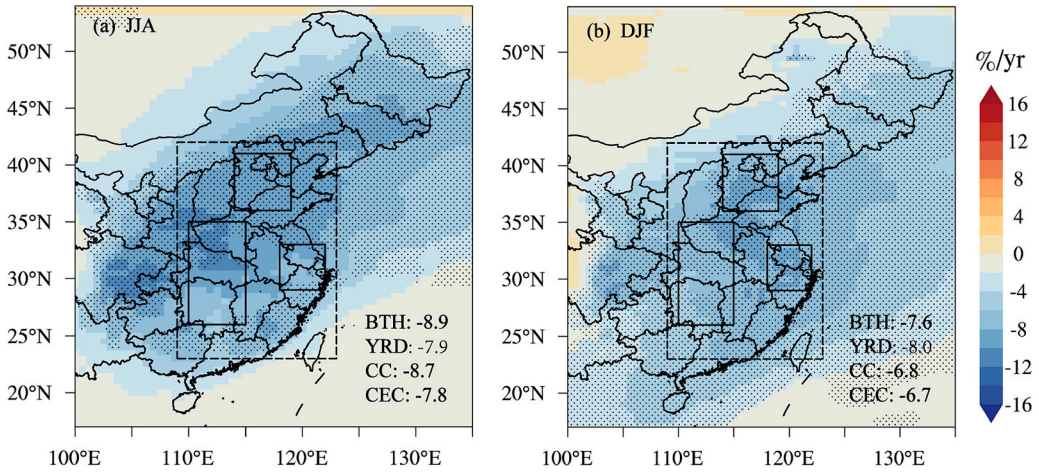

Fig. 6. Emission-driven relative trends in seasonal AOD over 2013–2020 simulated by the GEOS-Chem model. The average relative trends for regions of interest are inserted.

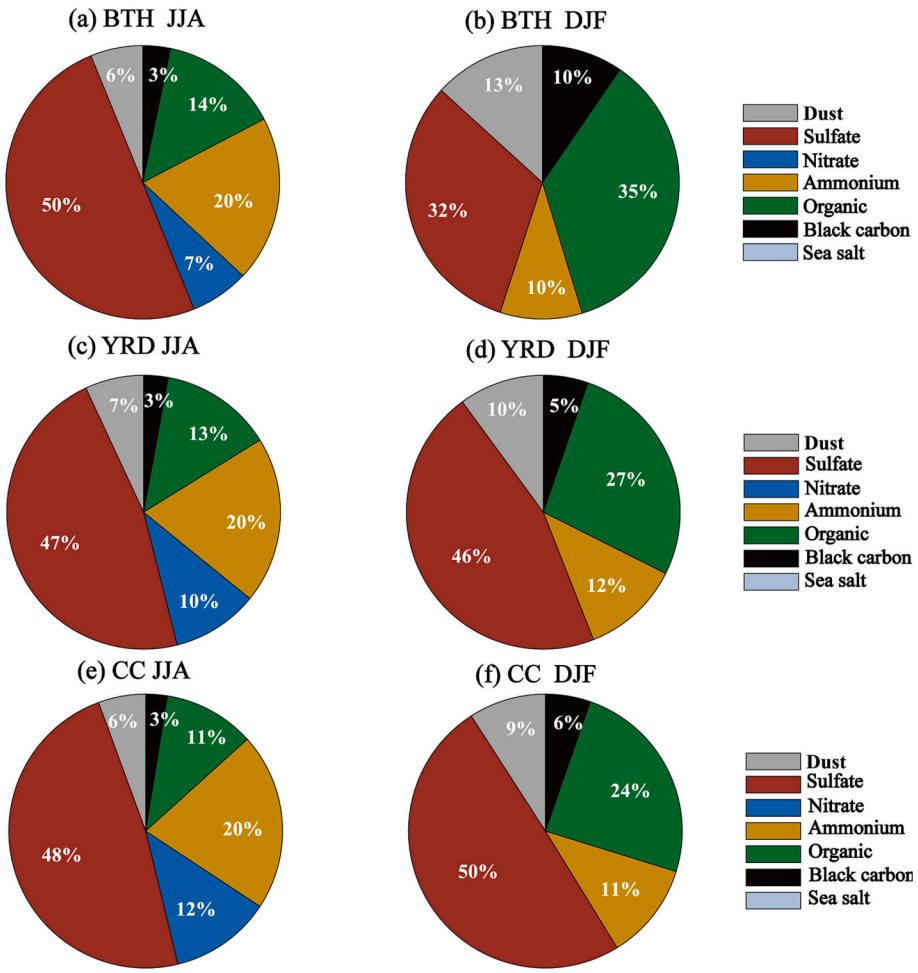

Fig. 7. Simulated contributions of aerosol components to relative trends of seasonal AOD in (a-b) Beijing-Tianjin-Hebei (BTH), (c-d) the Yangtze River Delta (YRD), and (e-f) Central China (CC) due to emission controls during 2013–2020.

ammonium was only half that in summer. In the meantime, the contributions of OA and BC doubled. The faster decrease of primary OA in winter than in summer (Lei et al., 2021; Li et al., 2023) may account for the seasonal variation of OA contribution. Observational study shows that winter OA decreased by 45.6 μg/m^3 from 2013 to 2020 in Beijing, whereas sulfate decreased by only 16.6 μg/m^3 (Lei et al., 2021). However, the high hygroscopicity of sulfate still resulted in a comparable contribution to the reduction of AOD with OA, as seen in the model. It is worth noting that nitrate aerosol can lead to a slight increase of AOD (<1 %/yr) in winter, despite its contribution of 7 %–12 % to the declining AOD trends in summer. NO_x reduction was more rapid in winter compared to summer (Table S1), indicating a more effective production of particulate nitrate in winter (Zhai et al., 2021a; Fu et al., 2020). Nitrogen oxidation ratio (NOR) is used to evaluate the efficiency of nitrate production. In winter, NOR exhibited a statistically significant increasing trend of 2–4 %/yr in different regions, but it demonstrated a decrease during summer. This indicates that variations in chemical reactions may lead to the seasonality in nitrate contribution to AOD trends.

Furthermore, when assessing the contributions that incorporate meteorological effects (Fig. S7), it was found that meteorological conditions have a relatively minor influence on chemical components, except for the contribution of nitrate in the BTH region. Li et al. (2023) reported that meteorology affected more nitrate than other components in summer. In our study, in the BTH region, meteorological conditions contributed by 5 % to the decreasing trend of AOD from sulfate but 122 % for nitrate in winter. As such, the intensity of emission control and the hygroscopicity played a decisive role in the 2013–2020 trends of AOD from sulfate, ammonium, OA, and BC, while chemical reactions and meteorological variations were more important for nitrate. Considering the lower dependency of nitrate on the wind (Li et al., 2023), we compared the regional average variations in RH and temperature with AOD from nitrate in BTH. The correlation between RH and AOD from nitrate was 0.81 in winter (Fig. S8) and the correlation with temperature was only 0.34, highlighting the dominant role of RH in nitrate AOD variations.

3.3.2. *Drivers of 2013–2020 changes in aerosol vertical distribution*

Fig. 8 shows the vertical profiles of relative trends in AEC driven by 2013–2020 emission changes. The response of AEC to emission controls in different regions was consistent vertically. In summer, the trends of AEC exhibited rapid decline by more than −8.0 %/yr within the planetary boundary layer (PBL) but had a rapid deceleration above the PBL. In winter, the declining trends of AEC started to decelerate in the lower layers. Given that the BTH region experienced the greatest reduction in emissions during both seasons (Table S1), the declining trends by up to −10.9 %/yr in BTH were the fastest in the lower PBL. In addition to the intensity of emission reduction, the changes in aerosol vertical distribution were also modulated by the climatology of planetary boundary layer height (PBLH) and RH. The seasonal variation of PBLH was negligible in the YRD region as shown in Fig. 8b and e. The higher RH in summer contributed to a 1.1 times greater AEC decline in YRD compared to winter, even though the reduction in emissions was a little more rapid during winter. On the other hand, the BTH region exhibited the

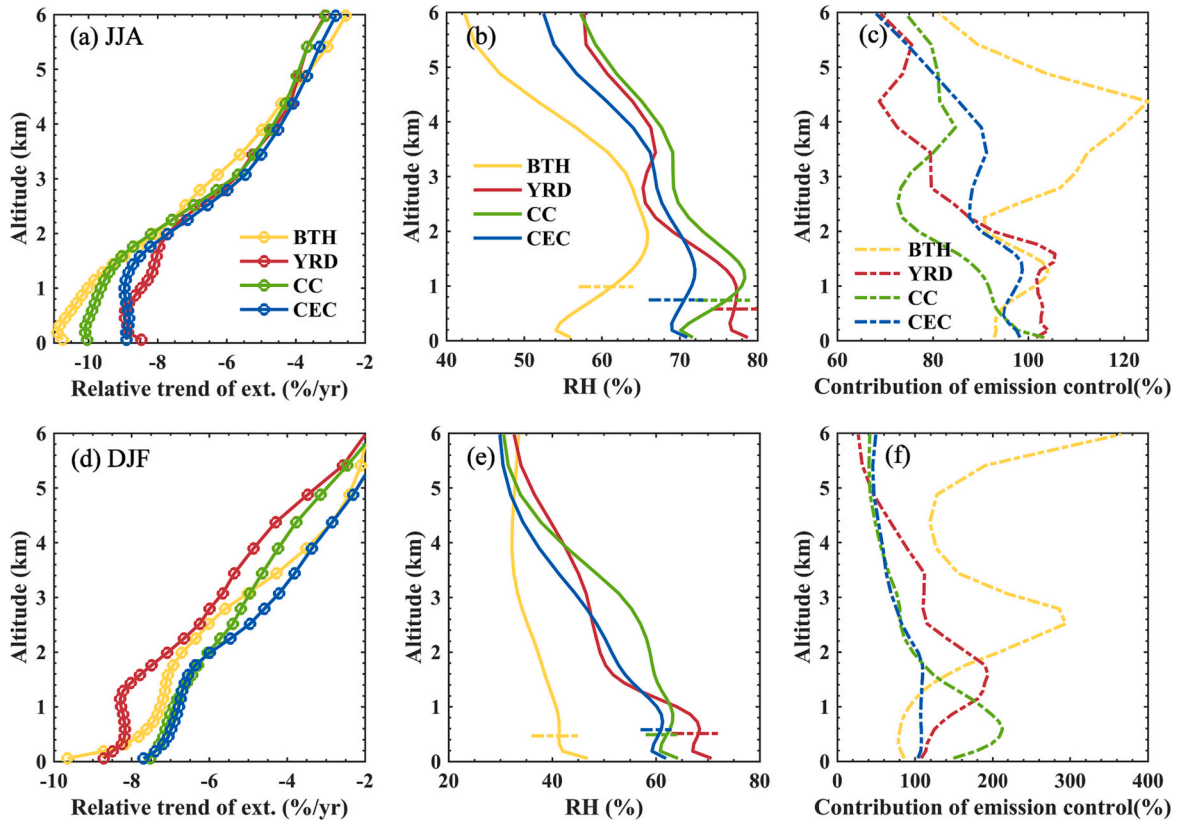

Fig. 8. Top panel (a-c): summertime profiles of emission-driven relative trends in aerosol extinction coefficient (a), multi-year mean relative humidity (RH) (b), and percentage contributions of emission control to the decreasing trends in aerosol extinction coefficient (c). Bottom panel (d-f) is the same as the top panel (a-c) except for wintertime profiles. The dashed lines in (b) and (d) show the climatology of planetary boundary layer heights in each region.

strongest seasonality in both AEC trends and PBLH, with the PBLH of 987 m in summer and 467 m in winter. In BTH, AEC declined faster in summer than in winter and reached a maximum factor of 1.4 between 450 m and 1 km, which can be attributed to the weaker PBL mixing above PBLH in winter.

Combined with the contributions of emission controls to the trends in AEC (Fig. 8c&f), we inferred that the seasonality of aerosol vertical distribution trends discussed in Section 3.2 was primarily influenced by meteorological conditions. In the BTH, CC, and YRD regions, the winter meteorological contribution experienced a transition aligned with the altitude exhibiting the slowest decrease in AEC at 2.8 km, 0.6 km, and 1.8 km, respectively, as illustrated in Fig. 3. Importantly, the effect of meteorological variations on the declining trends of column AOD was generally determined by the meteorological conditions within PBL, which is consistent with the findings proposed by Gui et al. (2021).

In Fig. 9, the contributions of aerosol components to column AOD trends were consistent with their contributions to AEC trends below 1 km. With the increase in altitude, the contribution of sulfate to the emission-driven trend of AEC increased initially below 2–3 km but subsequently decreased in all city clusters during both seasons. The contribution of ammonium decreased above 2 km, while dust exhibited an opposite trend. The contribution of dust increased significantly from 3 km in summer and 2 km in winter. Furthermore, during summer in the CC region, the contribution of OA in the upper layers exhibited the greatest increase, rising from 10 % at 2 km to 22 % at 6 km. Conversely, in winter in the BTH region, the contribution of OA experienced the most significant decrease, dropping by 12 % from 1 km to 6 km. The influence of nitrate on AEC trends varied greatly between seasons, like the contribution to column AOD. In summer, the contribution of nitrate to the decreasing trend of AEC was 9–13 % at 1 km, but it became unfavorable above 2.5–4.4 km. Nitrate caused a slight increase of AEC at all layers in YRD and CC regions during winter. However, nitrate contributed to a 7 % decreasing trend of AEC at the surface in the BTH region and turned unfavorable above 0.5 km. As we explained in the previous section, the more effective production of nitrate was the dominant factor. Besides, the impact of meteorological conditions on the contribution of different aerosol components to AEC is shown in Fig. S9. In general, meteorological conditions exert limited influence on the contribution of aerosol components to AEC at different altitudes during summer. However, the impact of meteorological conditions on sulfate contribution exhibits regional disparities during winter. In the CC region, the decrease in sulfate contribution attributed to meteorological factors declined from 10 % to 1 % with increasing altitude. In the YRD region, the reduction of sulfate contribution attributed to meteorology remained between 7 and 10 % below 2 km, and then the effect diminished. For other components, the impact of meteorological conditions shows less difference vertically.

4. Conclusions

In this study, we quantified the long-term trends of aerosol optical depth (AOD) and aerosol extinction coefficient (AEC) over China from 2013 to 2020 based on multiple observations and the GEOS-Chem model. With the good agreement between simulated and observed 8-year trends in aerosol vertical distribution, the effects of emission controls and meteorology were estimated by sensitivity simulations, and the role of aerosol components and meteorological factors was further identified.

The MODIS AOD exhibited a significant decreasing trend over 2013–2020 in major city clusters: Beijing-Tianjin-Hebei (BTH), the Yangtze River Delta (YRD), and Central China (CC). In summer, the relative trends of AOD ranged from −7.9 %/yr to −4.2 %/yr for the

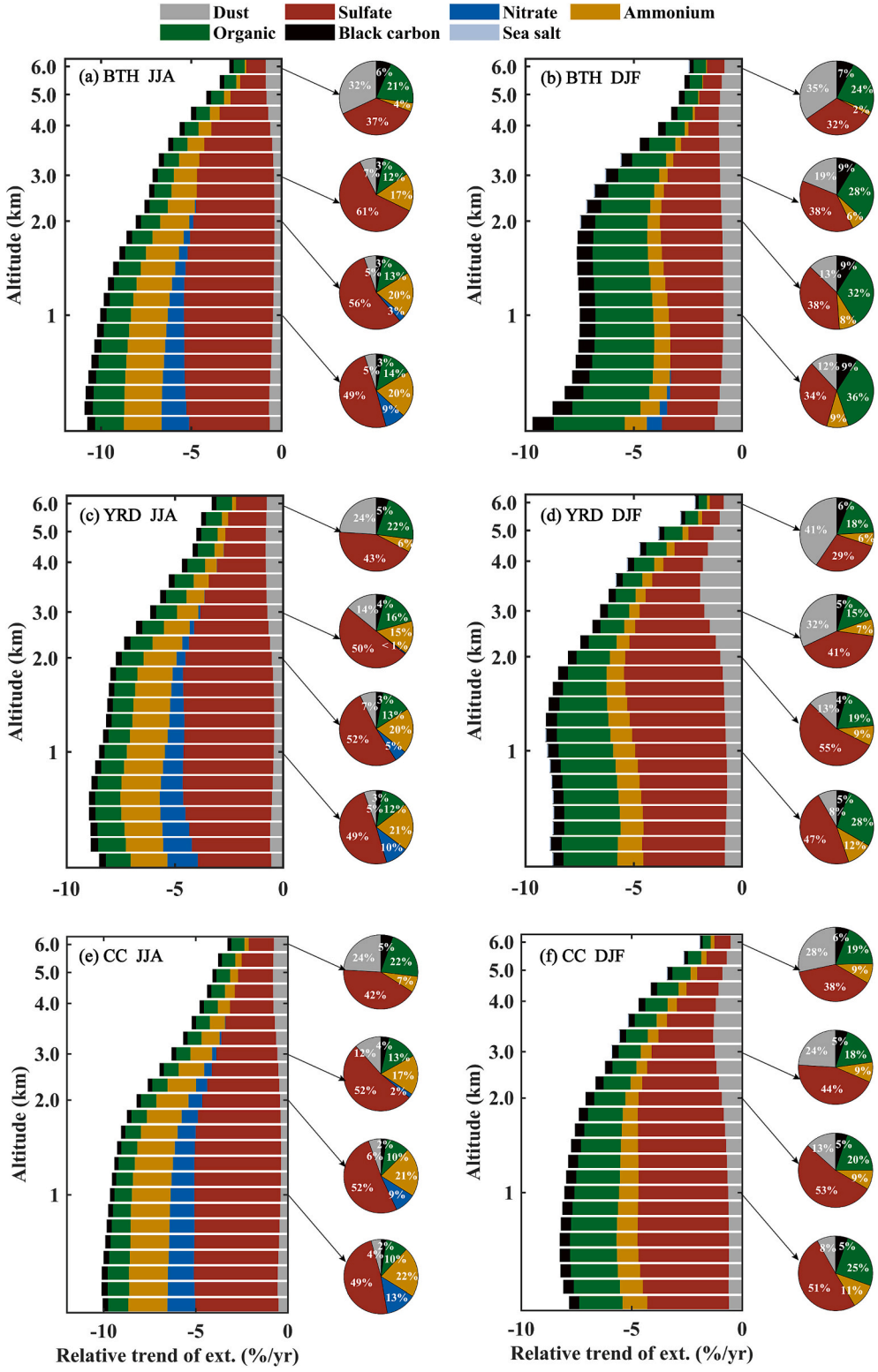

Fig. 9. Simulated contributions of aerosol components to relative trends of seasonal aerosol extinction coefficient in (a-b) Beijing-Tianjin-Hebei (BTH), (c-d) the Yangtze River Delta (YRD), and (e-f) Central China (CC) due to emission controls.

observation, while in winter, it was −6.1 %/yr to −5.8 %/yr. A seasonality of AOD trends was observed in the BTH and CC region, which was 1.2–1.3 times higher in summer. For the vertical AEC trends from CALIPSO, it was the fastest in the BTH region by −8.0 %/yr and the slowest in the CC region by −5.5 %/yr below ~1 km, then the trend slowed down as the altitude increased. These long-term trends and seasonality in AOD and vertical AECs were generally captured by the GEOS-Chem model. However, the relative trends from the model tended to be faster than observations, and the underestimation of mean AOD and AECs was possible due to the biased relative humidity.

Sensitivity simulations show that the substantial reduction of anthropogenic emissions was the primary driver of the 8-year AOD

decline. The emission-driven decreasing trends were − 7.8 %/yr in summer and −6.7 %/yr in winter for the whole CEC region. In summer, meteorological variations contributed by −2 % ~ 13 % to the AOD trends, while the meteorological variations were unfavorable in winter, with a contribution of −67 % ~ −2 %, which indicated the effect of meteorology cannot be neglected in the specific region. Vertically, meteorological conditions within the planetary boundary layer (PBL) are more important for column AOD. The intensity of emission reduction, as well as the climatology of local PBLH and relative humidity, were the dominant drivers of vertical distributions of AEC trends in response to emission controls.

To further understand the role of emission controls, the contributions from individual aerosol components were explored. During summer, the decline in AOD was primarily driven by the reduction of sulfate (47 %–50 %), followed by ammonium, and OA. However, in winter, both sulfate (32 %–50 %) and OA (24 %–35 %) played a significant role. Nitrate contributed to 7 % – 12 % of the declining AOD trends in summer but a slight increase of AOD in winter. Besides, the contributions of SNA aerosols to AEC trends decreased above 2–3 km, whereas primary aerosols contributed more. The contributions of sulfate, ammonium, OA, and BC were most influenced by the intensity of emission reduction and their hygroscopicity, while the contribution of nitrate was more sensitive to changes in chemical production and relative humidity.

In summary, compared with previous observational and statistical studies, the long-term modeling results in this work offer a unique insight into understanding aerosol vertical distribution changes both physically and chemically. In particular, due to the different seasonal changes in aerosol vertical distribution, effective control strategies should be formulated seasonally. Given the dominant contribution of SNA to the observed AOD decline in summer in the past decade, future attention should be paid to the reduction of OA with weaker hygroscopicity to realize the collaborative control of climate and pollution. In winter, efforts should be made to reduce the photochemical oxidation of NO_x via synchronized emission reduction of NO_x and VOCs, especially in the upper boundary layer. Notably, while the trends of aerosol vertical distribution from the model and observations were generally consistent, more observations, especially regarding the vertical distribution of aerosol and its components, are strongly needed for further studies. Moreover, accurate relative humidity inputs and locally applicable aerosol microphysical characteristics are also critical to the reliability of model results. Future investigation could be conducted to explore the climate effect induced by aerosol vertical distribution changes and their possible impacts on atmospheric photochemistry.

CRediT authorship contribution statement

Xi Chen: Writing – original draft, Formal analysis, Conceptualization. **Ke Li:** Writing – review & editing, Methodology, Conceptualization. **Ting Yang:** Formal analysis, Data curation. **Zhenjiang Yang:** Methodology, Formal analysis. **Xueqing Wang:** Software, Data curation. **Bin Zhu:** Writing – review & editing. **Lei Chen:** Writing – review & editing. **Yang Yang:** Writing – review & editing. **Zifa Wang:** Writing – review & editing. **Hong Liao:** Supervision.

Declaration of competing interest

The authors declare that they have no known competing financial interests or personal relationships that could have appeared to influence the work reported in this paper.

Data availability

The Level 3 monthly average MODIS AOD data are from https://ladsweb.modaps.eosdis.nasa.gov. The CALIPSO Level 2 aerosol profile product (V4.20) can be obtained from https://subset.larc.nasa.gov/calipso/login.php. Hourly surface $PM_{2.5}$ concentrations are from http://quotsoft.net/air. The MEIC anthropogenic emission inventory is from http://www.meicmodel.org. Other data are available on request from the first author (chenxi@nuist.edu.cn).

Acknowledgments

We would like to thank the support from the National Key Research and Development Program of China (2019YFA0606804, 2022YFE0136100), Jiangsu Carbon Peak and Neutrality Science and Technology Innovation fund (BK20220031), National Key Research and Development Program Young Scientists of China (2022YFC3704000), and the National Natural Science Foundation of China (42275122).

Appendix A. Supplementary data

Supplementary data to this article can be found online at https://doi.org/10.1016/j.scitotenv.2024.170485.

References

Chen, B., Song, Z., Pan, F., Huang, Y., 2022a. Obtaining vertical distribution of PM2.5 from CALIOP data and machine learning algorithms. Sci. Total Environ. 805, 150338. https://doi.org/10.1016/j.scitotenv.2021.150338.

Chen, B., et al., 2023a. Analysis of long-term trends in the vertical distribution and transport paths of atmospheric aerosols in typical regions of China using 15 years of CALIOP data. J. Geophys. Res. Atmos. 128 https://doi.org/10.1029/2022jd038066.

Chen, D., Liao, H., Yang, Y., Chen, L., Zhao, D., Ding, D., 2022b. Simulated impacts of vertical distributions of black carbon aerosol on meteorology and PM2.5 concentrations in Beijing during severe haze events. Atmos. Chem. Phys. 22, 1825–1844. https://doi.org/10.5194/acp-22-1825-2022.

Chen, X., Yang, T., Wang, H., Wang, F., Wang, Z., 2023b. Variations and drivers of aerosol vertical characterization after clean air policy in China based on 7-years consecutive observations. J. Environ. Sci. 125, 499–512. https://doi.org/10.1016/j.jes.2022.02.036.

Chen, Z., Chen, D., Kwan, M.-P., Chen, B., Gao, B., Zhuang, Y., Li, R., Xu, B., 2019. The control of anthropogenic emissions contributed to 80% of the decrease in PM2.5 concentrations in Beijing from 2013 to 2017. Atmos. Chem. Phys. 19, 13519–13533. https://doi.org/10.5194/acp-19-13519-2019.

Dang, R., Liao, H., 2019. Severe winter haze days in the Beijing-Tianjin-Hebei region from 1985 to 2017 and the roles of anthropogenic emissions and meteorology. Atmos. Chem. Phys. 19, 10801–10816. https://doi.org/10.5194/acp-19-10801-2019.

Deng, M., Chen, D., Zhang, G., Cheng, H., 2022. Policy-driven variations in oxidation potential and source apportionment of PM2.5 in Wuhan, central China. Sci. Total Environ. 853, 158255 https://doi.org/10.1016/j.scitotenv.2022.158255.

Ding, A.J., et al., 2016. Enhanced haze pollution by black carbon in megacities in China. Geophys. Res. Lett. 43, 2873–2879. https://doi.org/10.1002/2016gl067745.

Drury, E., et al., 2010. Synthesis of satellite (MODIS), aircraft (ICARTT), and surface (IMPROVE, EPA-AQS, AERONET) aerosol observations over eastern North America to improve MODIS aerosol retrievals and constrain surface aerosol concentrations and sources. J. Geophys. Res. Atmos. 115 https://doi.org/10.1029/2009JD012629.

Fu, X., Wang, T., Gao, J., Wang, P., Liu, Y., Wang, S., Zhao, B., Xue, L., 2020. Persistent heavy winter nitrate pollution driven by increased photochemical oxidants in northern China. Environ. Sci. Technol. 54, 3881–3889. https://doi.org/10.1021/acs.est.9b07248.

Guenther, A.B., Jiang, X., Heald, C.L., Sakulyanontvittaya, T., Duhl, T., Emmons, L.K., Wang, X., 2012. The model of emissions of gases and aerosols from nature version 2.1 (MEGAN2.1): an extended and updated framework for modeling biogenic emissions. Geosci. Model Dev. 5, 1471–1492. https://doi.org/10.5194/gmd-5-1471-2012.

Gui, K., et al., 2021. Three-dimensional climatology, trends, and meteorological drivers of global and regional tropospheric type-dependent aerosols: insights from 13 years (2007–2019) of CALIOP observations. Atmos. Chem. Phys. 21, 15309–15336. https://doi.org/10.5194/acp-21-15309-2021.

Guo, J., et al., 2016. Three-dimensional structure of aerosol in China: a perspective from multi-satellite observations. Atmos. Res. 178, 580–589. https://doi.org/10.1016/j.atmosres.2016.05.010.

Hersbach, H., et al., 2020. The ERA5 global reanalysis. Q. J. R. Meteorol. Soc. 146, 1999–2049. https://doi.org/10.1002/qj.3803.

Huang, X., Ding, A., Wang, Z., Ding, K., Gao, J., Chai, F., Fu, C., 2020. Amplified transboundary transport of haze by aerosol–boundary layer interaction in China. Nat. Geosci. 13, 428–434. https://doi.org/10.1038/s41561-020-0583-4.

Kang, H., Zhu, B., de Leeuw, G., Yu, B., van der A, R. J., and Lu, W., 2022. Impact of urban heat island on inorganic aerosol in the lower free troposphere: a case study in Hangzhou, China. Atmos. Chem. Phys. 22, 10623–10634. https://doi.org/10.5194/acp-22-10623-2022.

Kim, P.S., et al., 2015. Sources, seasonality, and trends of southeast US aerosol: an integrated analysis of surface, aircraft, and satellite observations with the GEOS-Chem chemical transport model. Atmos. Chem. Phys. 15, 10411–10433. https://doi.org/10.5194/acp-15-10411-2015.

Lei, L., et al., 2021. Long-term characterization of aerosol chemistry in cold season from 2013 to 2020 in Beijing, China. Environ. Pollut. 268, 115952 https://doi.org/10.1016/j.envpol.2020.115952.
Li, D., Xue, Y., Qin, K., Wang, H., Kang, H., Wang, L., 2022. Investigating the long-term variation trends of absorbing aerosols over Asia by using multiple satellites. Remote Sens. 14 https://doi.org/10.3390/rs14225832.
Li, J., Han, Z., 2016. Aerosol vertical distribution over east China from RIEMS-Chem simulation in comparison with CALIPSO measurements. Atmos. Environ. 143, 177–189. https://doi.org/10.1016/j.atmosenv.2016.08.045.
Li, J., Han, Z., Xie, Z., 2013. Model analysis of long-term trends of aerosol concentrations and direct radiative forcings over East Asia. Tellus Ser. B Chem. Phys. Meteorol. 65 https://doi.org/10.3402/tellusb.v65i0.20410.
Li, K., Jacob, D.J., Liao, H., Zhu, J., Shah, V., Shen, L., Bates, K.H., Zhang, Q., Zhai, S., 2019a. A two-pollutant strategy for improving ozone and particulate air quality in China. Nat. Geosci. 12, 906–910. https://doi.org/10.1038/s41561-019-0464-x.
Li, K., et al., 2021. Ozone pollution in the North China Plain spreading into the late-winter haze season. Proc. Natl. Acad. Sci. U. S. A. 118 https://doi.org/10.1073/pnas.2015797118.
Li, S., Zhang, L., Cai, K., Ge, W., Zhang, X., 2019b. Comparisons of the vertical distributions of aerosols in the CALIPSO and GEOS-Chem datasets in China. Atmospheric Environment: X 3. https://doi.org/10.1016/j.aeaoa.2019.100036.
Li, Y., et al., 2023. Significant reductions in secondary aerosols after the three-year action plan in Beijing summer. Environ. Sci. Technol. https://doi.org/10.1021/acs.est.3c02417.
Liao, T., Gui, K., Li, Y., Wang, X., Sun, Y., 2021. Seasonal distribution and vertical structure of different types of aerosols in southwest China observed from CALIOP. Atmos. Environ. 246, 118145 https://doi.org/10.1016/j.atmosenv.2020.118145.
Lin, J., Li, J., 2016. Spatio-temporal variability of aerosols over East China inferred by merged visibility-GEOS-Chem aerosol optical depth. Atmos. Environ. 132, 111–122. https://doi.org/10.1016/j.atmosenv.2016.02.037.
Liu, C., Huang, J., Hu, X.-M., Hu, C., Wang, Y., Fang, X., Luo, L., Xiao, H.-W., Xiao, H.-Y., 2021. Evaluation of WRF-Chem simulations on vertical profiles of PM2.5 with UAV observations during a haze pollution event. Atmos. Environ. 252, 118332 https://doi.org/10.1016/j.atmosenv.2021.118332.
Liu, Y., Wang, M., Yue, M., Qian, Y., 2023. Distinct seasonality in aerosol responses to emission control over northern China. J. Geophys. Res. Atmos. 128 https://doi.org/10.1029/2022jd038377.
Lu, W., Zhu, B., Liu, X., Dai, M., Shi, S., Gao, J., Yan, S., 2023. The influence of regional transport on the three-dimensional distributions of black carbon and its sources over eastern China. Atmos. Environ. 297, 119585 https://doi.org/10.1016/j.atmosenv.2023.119585.
Ma, X., Yu, F., 2014. Seasonal variability of aerosol vertical profiles over east US and West Europe: GEOS-Chem/APM simulation and comparison with CALIPSO observations. Atmos. Res. 140-141, 28–37. https://doi.org/10.1016/j.atmosres.2014.01.001.
Ma, Y., Jin, Y., Zhang, M., Gong, W., Hong, J., Jin, S., Shi, Y., Zhang, Y., Liu, B., 2021. Aerosol optical properties of haze episodes in eastern China based on remote-sensing observations and WRF-Chem simulations. Sci. Total Environ. 757, 143784 https://doi.org/10.1016/j.scitotenv.2020.143784.
Ma, Y., et al., 2022. How do aerosols above the residual layer affect the planetary boundary layer height? Sci. Total Environ. 814, 151953 https://doi.org/10.1016/j.scitotenv.2021.151953.
Miao, R., et al., 2020. Model bias in simulating major chemical components of PM2.5 in China. Atmos. Chem. Phys. 20, 12265–12284. https://doi.org/10.5194/acp-20-12265-2020.
Prospero, J.M., Barkley, A.E., Gaston, C.J., Gatineau, A., Campos y Sansano, A., and Panechou, K., 2020. Characterizing and quantifying African dust transport and deposition to South America: implications for the phosphorus budget in the Amazon Basin. Glob. Biogeochem. Cycles 34, e2020GB006536. https://doi.org/10.1029/2020GB006536.
Qi, L., Zheng, H., Ding, D., Wang, S., 2022. Effects of Anthropogenic Emission Control and Meteorology Changes on the Inter-Annual Variations of PM2.5-AOD Relationship in China. https://doi.org/10.3390/rs14184683.
Reddy, K.R.O., Zhang, X., Bi, L., 2019. Seasonal aerosol variations over a coastal city, Zhoushan, China from CALIPSO observations. Atmos. Res. 218, 117–128. https://doi.org/10.1016/j.atmosres.2018.11.011.
Shao, T., Wang, P., Yu, W., Gao, Y., Zhu, S., Zhang, Y., Hu, D., Zhang, B., Zhang, H., 2023. Drivers of alleviated PM2.5 and O3 concentrations in China from 2013 to 2020. Resour. Conserv. Recycl. 197 https://doi.org/10.1016/j.resconrec.2023.107110.
Sokolik, I.N., Soja, A.J., DeMott, P.J., Winker, D., 2019. Progress and challenges in quantifying wildfire smoke emissions, their properties, transport, and atmospheric impacts. J. Geophys. Res.-Atmos. 124, 13005–13025. https://doi.org/10.1029/2018JD029878.
Su, B., et al., 2020. Optical and physical characteristics of aerosol vertical layers over northeastern China. Atmosphere 11. https://doi.org/10.3390/atmos11050501.
Sun, Y., et al., 2021. Mapping the drivers of formaldehyde (HCHO) variability from 2015 to 2019 over eastern China: insights from Fourier transform infrared observation and GEOS-Chem model simulation. Atmos. Chem. Phys. 21, 6365–6387. https://doi.org/10.5194/acp-21-6365-2021.
Tan, W.S., et al., 2023. Soil emissions of reactive nitrogen accelerate summertime surface ozone increases in the North China Plain. Environ. Sci. Technol. https://doi.org/10.1021/acs.est.3c01823.
Uno, I., et al., 2009. Asian dust transported one full circuit around the globe. Nat. Geosci. 2, 557–560. https://doi.org/10.1038/NGEO583.
Wang, G., Deng, T., Tan, H., Liu, X., Yang, H., 2016. Research on aerosol profiles and parameterization scheme in Southeast China. Atmos. Environ. 140, 605–613. https://doi.org/10.1016/j.atmosenv.2016.06.027.
Wang, H., Yang, T., Wang, Z., 2020. Development of a coupled aerosol lidar data quality assurance and control scheme with Monte Carlo analysis and bilateral filtering. Sci. Total Environ. 728, 138844 https://doi.org/10.1016/j.scitotenv.2020.138844.
Wang, J., et al., 2017. Particulate matter pollution over China and the effects of control policies. Sci. Total Environ. 584-585, 426. https://doi.org/10.1016/j.scitotenv.2017.01.027.
Wang, X., 2023. Historical air quality data in China. http://quotsoft.net/air last access: 31 August.
van der Werf, G.R., et al., 2017. Global fire emissions estimates during 1997–2016. Earth Syst. Sci. Data 9, 697–720. https://doi.org/10.5194/essd-9-697-2017.
Wu, J.-B., Wang, Z., Wang, Q., Li, J., Xu, J., Chen, H., Ge, B., Zhou, G., Chang, L., 2017. Development of an on-line source-tagged model for sulfate, nitrate and ammonium: A modeling study for highly polluted periods in Shanghai, China. Environ. Pollut. 221, 168–179. https://doi.org/10.1016/j.envpol.2016.11.061.
Xiao, Q., Geng, G., Xue, T., Liu, S., Cai, C., He, K., Zhang, Q., 2022. Tracking PM(2.5) and O(3) pollution and the related health burden in China 2013-2020. Environ. Sci. Technol. 56, 6922–6932. https://doi.org/10.1021/acs.est.1c04548.
Yang, Y., Liao, H., Lou, S., 2016. Increase in winter haze over eastern China in recent decades: roles of variations in meteorological parameters and anthropogenic emissions. J. Geophys. Res.-Atmos. 121, 13050–13065. https://doi.org/10.1002/2016JD025136.
Yu, P., et al., 2019. Black carbon lofts wildfire smoke high into the stratosphere to form a persistent plume. Science 365, 587–590. https://doi.org/10.1126/science.aax1748.
Zhai, S., et al., 2021b. Relating geostationary satellite measurements of aerosol optical depth (AOD) over East Asia to fine particulate matter (PM2.5): insights from the KORUS-AQ aircraft campaign and GEOS-Chem model simulations. Atmos. Chem. Phys. 21, 16775–16791. https://doi.org/10.5194/acp-21-16775-2021.
Zhai, S., et al., 2021a. Control of particulate nitrate air pollution in China. Nat. Geosci. 14, 389–395. https://doi.org/10.1038/s41561-021-00726-z.
Zhang, L., et al., 2015. Source attribution of particulate matter pollution over North China with the adjoint method. Environ. Res. Lett. 10 https://doi.org/10.1088/1748-9326/10/8/084011.
Zhang, Q., et al., 2019. Drivers of improved PM2.5 air quality in China from 2013 to 2017. Proc. Natl. Acad. Sci. U. S. A. 116, 24463–24469. https://doi.org/10.1073/pnas.1907956116.
Zhang, Y., et al., 2017. Top-of-atmosphere radiative forcing affected by brown carbon in the upper troposphere. Nat. Geosci. 10, 486. -+. https://doi.org/10.1038/NGEO2960.
Zheng, B., et al., 2018. Trends in China's anthropogenic emissions since 2010 as the consequence of clean air actions. Atmos. Chem. Phys. 18, 14095–14111. https://doi.org/10.5194/acp-18-14095-2018.